APPLICATION OF A NAVIER-STOKES CODE TO THE SIMULATIONS OF HIGH-LIFT DEVICES USING UNSTRUCTURED GRIDS

João Alves de Oliveira Neto*, Edson Basso and João Luiz F. Azevedo****
***Instituto Tecnológico de Aeronáutica, CTA/ITA/EEC-I, **Instituto de Aeronáutica e Espaço, CTA/IAE/ ALA**

Keywords: *CFD, High-Lift Devices, Aerodynamic Coefficients, Turbulence Models*

Abstract

The purpose of the present paper is to perform a study of high-lift configurations using CFD simulations. Such study is attempt to establish guidelines for the analysis and design of such devices through computational aerodynamics techniques. The study is motivated by the realization that an increased understanding of high-lift systems plays in important role in designing the high-performance transport aircraft. Studies ranged from 2-D simulations based on the steady state Euler equations coupled to the boundary layer equations, to simulations of the Reynolds-averaged Navier Stokes equations for 2-D configurations.

1 Introduction

The design of an optimized high-lift system is an important part of the development of a modern transport aircraft. The manufacturers must make simple yet efficient high-lift designs and, in particular, they must avoid having to make large expensive changes in a late project stage. The cost and Reynolds number scaling problems involved in the optimization of slat and flap positions by wind tunnel tests is a strong driver in the effort to develop CFD tools which can be used in the design process. This paper describes one step on the road to establish CFD analysis tools for high-lift aerodynamics, by developing methods and performing validation of 2-D high-lift analysis capabilities.

High-lift flows are inherently three-dimensional and a complete study should include the modeling and analysis of such effects. However, several aspects of high-lift flows may be understood by simplified two-dimensional analysis. For instance, viscous interaction effects are responsible for the most important limiting aspects of such flows. The confluence of the wake of one element with the suction side boundary layer of the following elements plays an important role in determining maximum lift. Massive flow separation on one or more of the elements may, depending on operational condition, set the maximum lift which can be obtained. The fact that many portions of the flow develop in strong adverse pressure gradients increases the modeling difficulties. The knowledge of turbulence development in adverse pressure gradients is much less developed than it is for zero pressure gradient flows. Most turbulence models used in Reynolds averaged computational methods are calibrated in zero pressure gradient flows, with more or less *ad hoc* modifications to account for the development of turbulence in adverse pressure gradient regions. Moreover, many effects in high-lift flows are governed by the detailed transition process. This can be quite different in wind tunnel tests taken at lower Reynolds number compared to the flight situation. The numerical calculation of all of these phenomena must also address the

subjects of grid refinement and grid independent solutions. In any event, even with the known limitations of 2-D analysis in mind, the results are still quite useful in the initial design phase and to increase the understanding of the governing flow phenomena.

In this context, the purpose of the present work is to perform a systematic analysis of several physical and numerical aspects which can influence the quality of simulations of high-lift flows. The first aspect to be addressed concerns the fundamental question in numerical calculations associated with grid refinement and its effects on the flow solution obtained. Mesh independent results may be difficult to achieve, especially for such complex flows as usually found in high-lift systems. In any event, such mesh independency must be sought and the paper will describe an approach towards such goal. The paper will also address the effect of turbulence models on the quality of the high-lift solutions. The present effort will only consider 2-D configurations, in an attempt to reduce the computational costs, due to the need of discretizing complex 3-D flows, and use the available mesh points to explore more subtle aspects of the 2-D results.

2 High-Lift Devices: Geometry and Grid Generation

Geometry of the 2D profiles is obtained in coordinate files and the trailing edges are not collapsed in either element. Mesh generation is performed with the ANSYS ICEM CFD code [1]. Several parameter variations are performed in order to check their influence on the final CFD result. The parameter studies performed include the analysis of effects such as farfield distance, boundary layer refinement general, grid refinement and mesh topology. The geometries considered in the present effort include a NLR 7301 is supercritical airfoil/flap configuration with 32% chord flap [2]. This geometry, considering a 20 deg. flap deflection and with a 1.3% gap, is show in Fig. 1. The NHLP-2D airfoil is again a supercritical airfoil with high-lift devices, including a 12.5% leading-edge slat and a 33% single-slotted

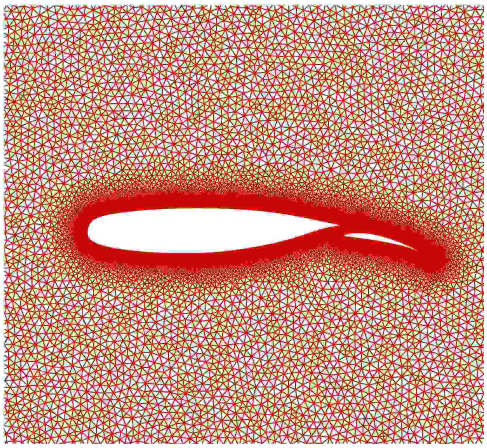

Fig. 1 Mesh over the NLR 7301 airfoil.

flap [3]. For the results shown here, the slat and flap are deflected 25 and 20 deg., respectively, as shown in Fig. 2.

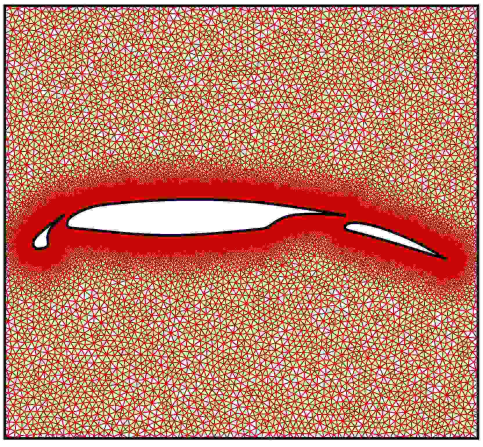

Fig. 2 Mesh over the NHLP-2D airfoil.

An overall consideration on grid generation for high-lift design, based on the present analyse, states that a hundred times the profile chord is the standard measure used for the farfield distance. Boundary layer has a crucial importance in the final result and shall be discretized according to the needs of the flow conditions once the boundary layer parameters are defined, a grid topology may be created to better define the boundary layer limits. The hexa/quad grid is the most indicated for high-lift CFD analysis, but one must respect the grid topology in order to preserve the mesh quality. Not surprisingly, grid sizes tended to increase

in density from less than 50.000 points to about triple such size as the decade advanced. Many independent grid studies seemed to suggest that 50.000 points may be sufficient to resolve surface pressures, but flow field quantities such as velocity profiles require significantly more grid points. Some estimates indicate that, at least, 100.000 to 200.000 elements are required, unless a scheme with higher order spatial accuracy is employed. Grid issues tendo to still remain very important in general. Those references that exercise the greatest care in ensuring high-quality, sufficiently refined grids with an accurate representation of the wind tunnel geometry tended to produce the best correlations with experiment.

Underresolution in key areas, such as wakes, can lead to overdissipation and incorrect conclusions. Moreover, for 2-D computations, it is important to have a farfield grid extent of, at least, 50 to 60 chords or, otherwise, special farfield boundary condition treatment is required in order to accurately predict drag. The inclusion of tunnel walls in the computations appears to be increasingly important at higher angles of attack. A consistent method for studying convergence of the computed solutions with increasing grid density is an important pre-requisite for validating an automated CFD analysis procedure. Consistency of the grid system is difficult to achieve when analyzing high-lift flows. The difficulty arises out of the need to ensure sufficient grid density and smoothness in other areas. The problem is further compounded by a lack of guidelines regarding grid resolution requirements for the complex flow physics involving disparate length scales that arise in flowfields over high-lift configurations.

3 Flow Solution Method

3.1 Simulation Conditions

Usually, the solving step in the simulation process consumes most of the computational time. In order to estimate the number of simulations and flow conditions required for a given study, and hence the necessary computational, it is interesting to have some idea of the expected results. In the early stages of the preliminary design of an airplane, some of the aerodynamic coefficients are already know due to certain airplane performance figures that have to be achieved. In particular, the high-lift devices are intrinsically connected with the landing and the take-off performance. These two phases of the airplane mission are very important due to their operational implications. An overestimated take-off C_{lmax} implicates in limitations in the maximum weight to take-off, or the need for an longer runway. In the same way, an overestimated landing C_{lmax} implicates in the necessity for a longer track. The aerodynamic coefficients are directly influenced by the flow conditions, i.e., speed, altitude and temperature, angle of attack and individual displacement parameters of the high-lift elements, i.e., gaps and overlaps. The aerodynamicist must select the configuration for which maximum lift coefficient is achieved, and to do so the number of simulations, combining all the cited parameters and conditions can grow out of limit on design time and costs to compute all the possible combinations. A solution must be found in order to reduce the simulation time.

3.2 MSES Code

The MSES code [4] is a two dimensional analysis, design and optimization framework for multi-element airfoil sections. It is based on the steady state, conservative, Euler equations. The Euler equations are used to describe the inviscid part of the flow. The assumption that the viscous part is restricted to a thin boundary layer and wake is made, and the viscous part is described with the boundary layer theory given by the integrated Prandtl boundary layer equations [5]. The equations are discretized in an intrinsic mesh, where one set of coordinate lines correspond to the streamlines around the body. With this procedure the number of unknowns per grid node is reduced from four to two because the continuity equation and the energy equation can be replaced by the simple condition of constant mass flux and constant stagnation enthalpy along each stream-

tube. The Newton method is used for solving the system of nonlinear equations. Simulations are performed quickly and the aerodynamic coefficients are obtained. A comparison of experimental data and the MSES code results are presented in the present paper.

3.3 CFD++ Code

The CFD++ code [6] allows easy treatment of meshes for complex geometries mainly due to its integration of structured, unstructured and multiblocks grids. Its flexibility allows the use of various elements within the same mesh such as hexahedral, triangular prism and tetrahedral elements in 3-D. However, as usual with RANS simulations for such high Reynolds number flows, the addition of turbulence models is required in order to capture the correct turbulent transport. In the present paper, both the Spalart-Allmaras (SA) one-equation and Menter SST (SST) two-equation models are used.

4 Results and Discussion

4.1 NLR 7301 airfoil

The NLR 7301 is a supercritical airfoil/flap configuration with 32% chord flap. The current simulations consider a $\delta_f = 20^o$ flap deflection [2]. In this present study, two different configurations are evaluated. The first analysis is performed for the configuration with a flap gap of 1.3% and the second one with the flap gap of 2.6%. In the present simulations, a triangular and quadrilateral grid with 200.229 elements is used. The gap is defined as the radius of the circumference centered in the trailing edge of the main element and tangent to the flap profile at a certain point. This point of tangency is defined by the overhang, which is held at a constant value of 5.3% for both test cases here considered. It is worth mentioning that the gap and the overhang are defined as a percentage of the nominal profile cruise chord. Simulations of subsonic flow over the NLR 7301 profile are performed with freestream Mach number $M_\infty = 0.185$ and Re = 2.51 x 10^6, considering both inviscid and viscous flow options. In these simulations, both SA and SST turbulence models are exercised, as a form of comparing their results.

The lift coefficient as a function of angle of attack can be observed in detail in Fig. 3. This figure compares results obtained with the SA and SST turbulence models, the MSES code, and the experimental data. Comparison of experimental and calculated lift coefficients also shows good agreement which is a clear indication of the good quality of the results that can be obtained with the CFD++ numerical tool. One can observe in Fig. 3 that the numerical lift curves compare very well with experimental data, except for the MSES code. The lift coefficient as a function of angle

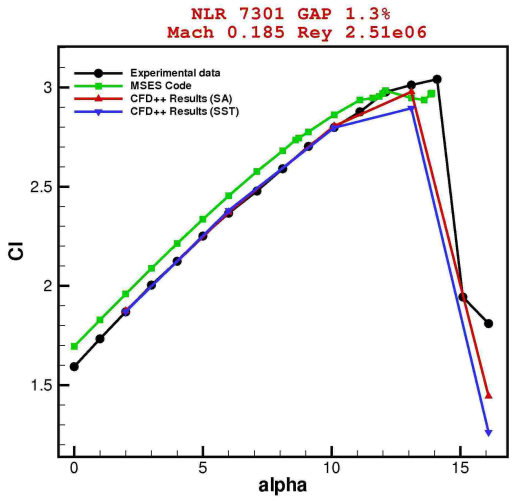

Fig. 3 The lift coefficient as a function of the angle of attack with Mach number 0.185 for the NLR 7301 with 1.3% gap.

of attack can be observed in detail in Fig. 4 for the NLR 7301 airfoil with 2.6% gap. This figure compares results obtained with the SA and SST turbulence models, the MSES code, and the experimental data. In Figs. 3 and 4, as in the NLR 7301 profile (1.3% and 2.6% gap) study the MSES code results also present an overprediction of lift coefficient for this geometry. The differences in the lift coefficient as a function of angle of attack curve seem to have been more accentuated. For an perfect match with the experimental results, all the complex physics has to be

perfectly captured, including the flow features at the cove of the main element, and the interactions between the free shear layer of the main element and the boundary layer of the flap. The MSES code presents a good capability to effectively reproduce the experimental data in the linear range. The limitations presented in the nonlinear region are intrinsic to the MSES formulation [7], as well the lack of a better control in relation to the mesh generation. This verification does not take away the merits of the code since, even other numerical codes with a much more complex formulation present the same difficulty in capturing the aerodynamic coefficients with accuracy.

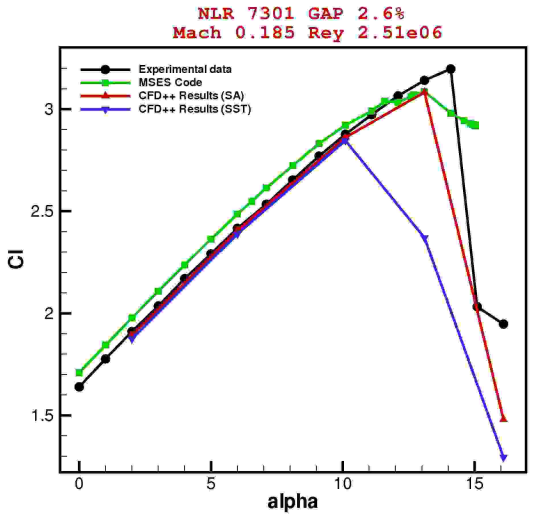

Fig. 4 The lift coefficient as a function of the angle of attack with Mach number 0.185 for the NLR 7301 with 2.6% gap.

The present paper still contemplated the study of numerical results including lift and drag coefficients for the NLR 7301 airfoil with 1.3% gap, and the comparison with experimental data. In the reality, 72 cases had been twirled approximately, that is, two aerodynamic coefficients with three models of turbulence and five different angle of attacks had been calculated. In this new analysis, three meshes unstructured with different refinements are used. These meshes are nominated meshes initial, medium and final. These meshes have rectangular topologies and possess the position of the situated external border the 100 chords of the profile. To assure a good quality in all the meshes, had been generated meshes unstructured composed for hexaedros and details of the grids used in the simulations can be seen in the Tab. 1.

Table 1 Details of computational grids pertinent of NLR 7301 airfoil with 1.3% gap.

Grid	Initial	Medium	Final
Elements total	156.731	382.997	866.391

The first grid used for the aerodynamic calculation has a total of 156.731 elements. Simulations of subsonic flow over the NLR 7301 profile are performed with freestream Mach number $M_\infty = 0.185$ and Re = 2.51 x 10^6, considering viscous formulation. In these simulations, both SA, SST and $k-\varepsilon$ realizable turbulence models are exercised, as a form of comparing their results. The lift coefficient as a function of the angle of attack can be observed, in details, in the Fig. 5, that in this case that it were calculated with the initial grid. This figures compares the turbulence

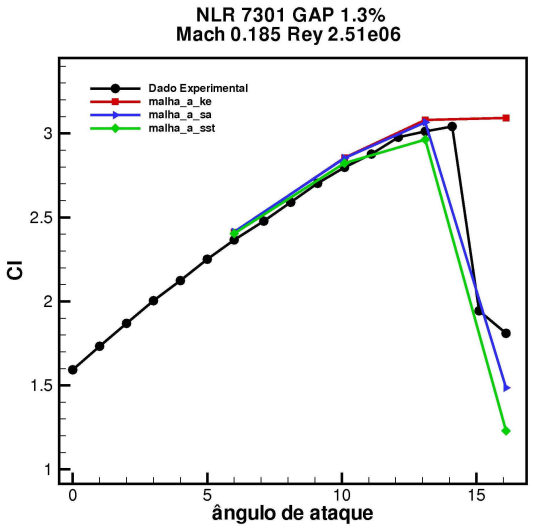

Fig. 5 The lift coefficient as a function of the angle of attack with Mach number 0.185 for the NLR 7301 with 1.3% gap using initial grid.

models presented in that analysis with the experimental data. It is possible observe that the SA and SST turbulence models also shows a good result in comparison with the experimental results. Already the $k-\varepsilon$ turbulence model achievable not obtain a good agreement in the nonlinear region of the flow in question. In the Tab. 2 we be able to verify in detail the lift coefficient regarding the of angle of attack for each case rolled.

Table 2 Values of the lift coefficients in case of the initial grid.

Initial grid							
k - ε		SA		SST		Experimental	
Cl	alfa	Cl	alfa	Cl	alfa	Cl	alfa
2.412	6.0	2.414	6.0	2.404	6.0	2.366	6.0
2.855	10.1	2.853	10.1	2.823	10.1	2.798	10.1
3.080	13.1	3.066	13.1	2.963	13.1	3.012	13.1
3.09255	16.1	1.486	16.1	1.230	16.1	1.810	16.1

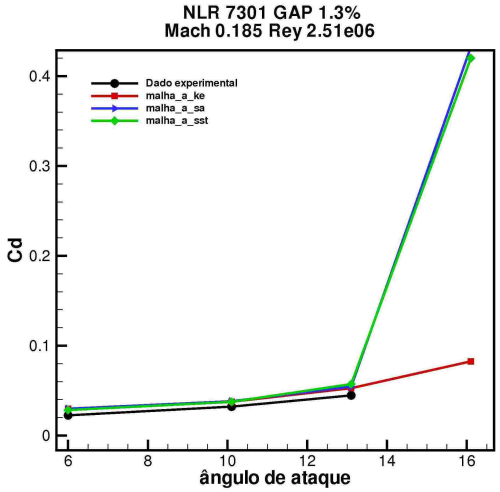

Fig. 6 The drag coefficient as a function of the angle of attack with Mach number 0.185 for the NLR 7301 with 1.3% gap using initial grid.

In the Fig. 6, is possible observe the drag coefficient as a function of the angle of attack, computed with the initial grid. In the linear region of the drag coefficient curve, the results with the SA and SST turbulence models presented a good result, including in the nonlinear region. Unfortunately, the $k-\varepsilon$ realizable turbulence model did not behave as expected in the region of high angle of attack. In the reality, this incapacity of the $k-\varepsilon$ realizable model achievable of do a forecast of the separation of the flow is associated to the absence of answer to the curvature of the flow. In the Tab. 3 is possible verify in detail the drag coefficient in relation to the angle of attack for each case calculated.

Table 3 Values of the drag coefficients in case of the initial grid.

Initial grid							
k - ε		SA		SST		Experimental	
Cd	alfa	Cd	alfa	Cd	alfa	Cd	alfa
0.02975	6.0	0.02989	6.0	0.02839	6.0	0.0225	6.0
0.03761	10.1	0.03817	10.1	0.03749	10.1	0.0322	10.1
0.05273	13.1	0.05443	13.1	0.05727	13.1	0.0447	13.1
0.08255	16.1	0.4323	16.1	0.42	16.1		

To second grid utilized for the calculation of the aerodynamic coefficients has a total of 382.997 elements. Once again, simulations of subsonic flow over the NLR 7301 profile are performed with freestream Mach number $M_\infty = 0.185$ and Re = 2.51 x 10^6, considering viscous formulation. In these simulations, both SA, SST and $k-\varepsilon$ realizable turbulence models are exercised, as a form of comparing their results. The lift coefficient as a function of the angle of attack can be observed in detail in the Fig. 7. In This figures, the SA turbulence model overestimates the curve of Cl versus alpha of the experimental result, but the calculation of Cl obtained convergence. In case of the SST model, the calculation of the lift coefficient, when the angle of attack is 12.1^o was not satisfactory, therefore the value of Cl not obtain convergence. Beyond this, the value of the $k-\varepsilon$ turbulence model achievable not obtain good agreement with the experimental results, ignoring the region of not linearity near to the region of the stall. In the Tab. 4 is possible verify in detail the curve of the lift coefficient as a function of the angle of attack for each case rolled.

In the Fig. 8 is possible observe the drag coefficient as a function of the angle of attack, computed with the medium grid. In the linear region of the drag coefficient curve, the results with

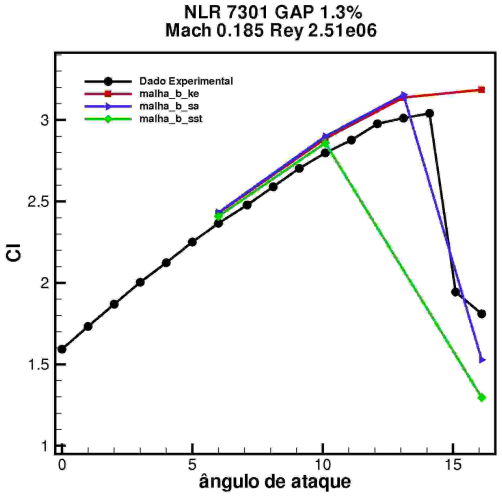

Fig. 7 The lift coefficient as a function of the angle of attack with Mach number 0.185 for the NLR 7301 with 1.3% gap using medium grid.

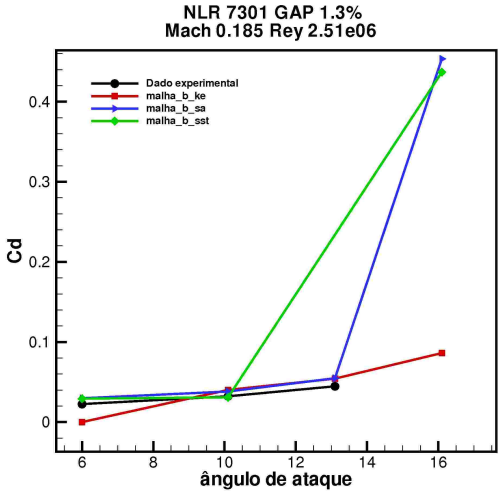

Fig. 8 The drag coefficient as a function of the angle of attack with Mach number 0.185 for the NLR 7301 with 1.3% gap using medium grid.

Table 4 Values of the lift coefficients in case of the medium grid.

Medium grid							
k - ε		SA		SST		Experimental	
Cl	alfa	Cl	alfa	Cl	alfa	Cl	alfa
2.429	6.0	2.432	6.0	2.409	6.0	2.366	6.0
2.886	10.1	2.900	10.1	2.859	10.1	2.798	10.1
3.138	13.1	3.155	13.1			3.012	13.1
3.18655	16.1	1.528	16.1	1.296	16.1	1.810	16.1

the SA and SST turbulence models presented a good result, including in the nonlinear regions, unless, in case of 12.1^o the angle of attack the value of the drag coefficient not obtain convergence in case of of the calculation with the SST model. In the Tab. 5 it is possible verify in detail the behavior of the drag coefficient regarding the angle of attack for each case calculated.

Table 5 Values of the drag coefficients in case of the medium grid.

Medium grid							
k - ε		SA		SST		Experimental	
Cd	alfa	Cd	alfa	Cd	alfa	Cd	alfa
0.03021	6.0	0.02976	6.0	0.02923	6.0	0.0225	6.0
0.04014	10.1	0.03820	10.1	0.03097	10.1	0.0322	10.1
0.05427	13.1	0.05478	13.1			0.0447	13.1
0.08618	16.1	0.4535	16.1	0.4369	16.1		

Unfortunately, the $k-\varepsilon$ realizable turbulence model achievable did not calculate as expected the drag coefficient in the region of high angle of attack. Once again, this deficiency of the $k-\varepsilon$ model achievable, of do a forecast of the detachment of the flow, is associated to the absence of answer to the curvature of the flow.

The third grid utilized for the calculation of the aerodynamic coefficients has a total of 866.391 volumes of control. Like this, the simulations are carried out with the freestream Mach number of 0.185 and Reynolds number of Re = 2.51 x 10^6 utilizing a formulation RANS. The curve Cl x α can be observed in details in the Fig. 9. Verifying this figure, the SA, SST and $k-\varepsilon$ tubulence models achievable overestimate the curve Cl x α of the experimental result. In case of the $k-\varepsilon$ model achievable, the calculation of the lift coefficient of when the angle of attack was of 6^o and 16.1^o, respectively, was not satisfactory, therefore the value of lift coefficient diverged in those values of α. In the Tab. 6 it is possible verify in detail the values of the lift coefficients as a function of the angle of attack for each case computed.

In the Fig. 10, is possible observe the drag coefficient as a function of the angle of attack, com-

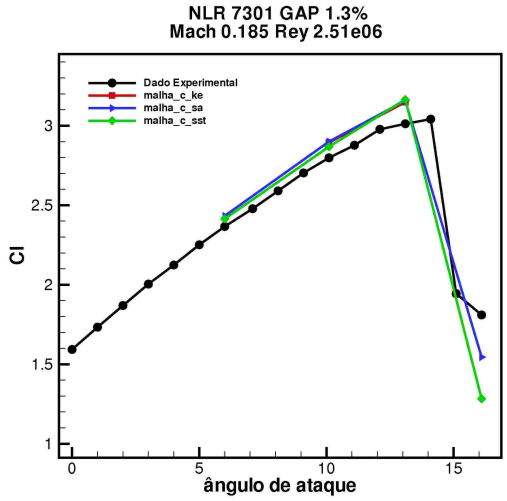

Fig. 9 The lift coefficient as a function of the angle of attack with Mach number 0.185 for the NLR 7301 with 1.3% gap using final grid.

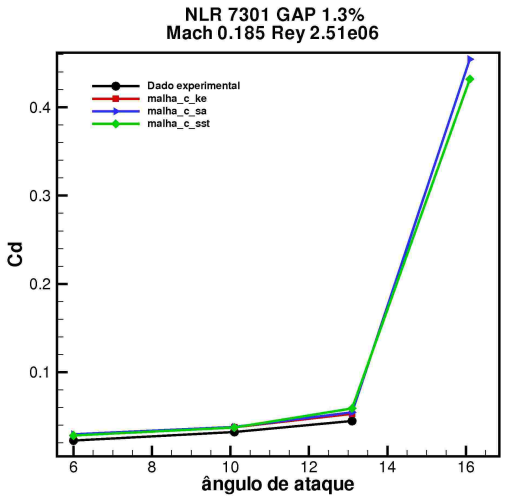

Fig. 10 The drag coefficient as a function of the angle of attack with Mach number 0.185 for the NLR 7301 with 1.3% gap using final grid.

Table 6 Values of the lift coefficients in case of the final grid.

Final grid							
k - ε		SA		SST		Experimental	
Cl	alfa	Cl	alfa	Cl	alfa	Cl	alfa
		2.433	6.0	2.414	6.0	2.366	6.0
2.894	10.1	2.900	10.1	2.868	10.1	2.798	10.1
3.148	13.1	3.157	13.1	3.164	13.1	3.012	13.1
		1.545	16.1	1.283	16.1	1.810	16.1

Table 7 Values of the drag coefficients in case of the final grid.

Malha final							
k - ε		SA		SST		Experimental	
Cd	alfa	Cd	alfa	Cd	alfa	Cd	alfa
		0.02964	6.0	0.02826	6.0	0.0225	6.0
0.03752	10.1	0.03795	10.1	0.03726	10.1	0.0322	10.1
0.05282	13.1	0.05448	13.1	0.05893	13.1	0.0447	13.1
		0.4545	16.1	0.432	16.1		

puted with the final grid. In the linear region of the drag coefficient curve, the results with all of the models of turbulence presented a good agreement including in the nonlinear region. Once again, had problem for the calculations in 6^o and 16.1^o of the angles of attack. In these cases, the calculation of the coefficient diverged for the $k-\varepsilon$ turbulence model achievable. Being like this, the $k-\varepsilon$ model achievable did not calculate as expected the drag coefficient in the region of high angle of attack. In the Tab. 7 it is possible verify details about the drag coefficients regarding the angle of attack for each case calculated.

4.2 NHLP-2D Airfoil

Wind tunnel data were measured for a two-dimensional supercritical airfoil with high-lift devices and the model designation is NHLP-2D [3]. The case selected for examination here is L1T2 which includes a 12.5%c leading-edge slat and a 33%c single slotted-flap, where c is the chord length of the nested configuration. The slat is located in the optimum position at an angle of 25 degrees and the flap angle is 20 degrees. This geometry, which is typical of a take-off configuration, is show in Fig. 2. The flow conditions for this case are freestream Mach number $M_\infty = 0.197$ and Re = 3.52 x 10^6, and an angle of attack of 4^o, considering both inviscid and viscous flow options. In these simulations, both SA and SST turbulence models are exercised, as a

form of comparing their results. In the present simulations, triangular and quadrilateral mesh is used with 148.014 elements. Locations along the chord in which total pressure profiles are indicated in Fig. 11.

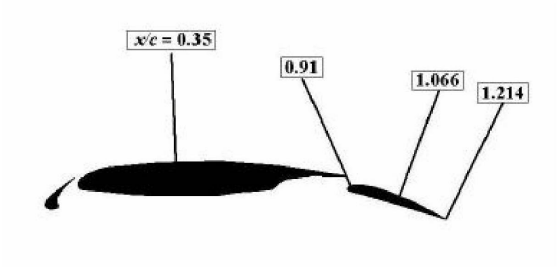

Fig. 11 Location of stations for which total pressure profiles are shown for the NHLP-2D airfoil.

The numerical results obtained by Morrison [8], using the Wilcox $k-\omega$ turbulence model, are also presented together with experimental data [3] for total pressure profile comparisons. The plot for x/c = 0.35, presented in Fig. 12, shows the slat wake and the boundary layer on the main element. The experimental data is sparse in the region of the slat wake and shows a narrower and weaker wake when compared to numerical results. The results of Morrison [8] predict a slat wake which is too large. The experiment shows more merging of the slat wake and main element boundary layer than the calculations show. There are differences in the two models, but they all fundamentally show a more distinct and boundary layer than the experimental.

The experimental profiles at all of the other downstream locations confirm the merging of the slat wake with element boundary layer, the slat wake is completely missing from the experimental total pressure profiles at the x/c = 0.91 and higher locations, presented in Fig. 13. All two of the models predict a distinct slat wake in the outer edge of the main element boundary layer all the way to the flap trailing edge (x/c = 1.214). The SA turbulence model shows the smallest wake at all the stations and the $k-\omega$ model shows the largest wake at all of the locations. The wake

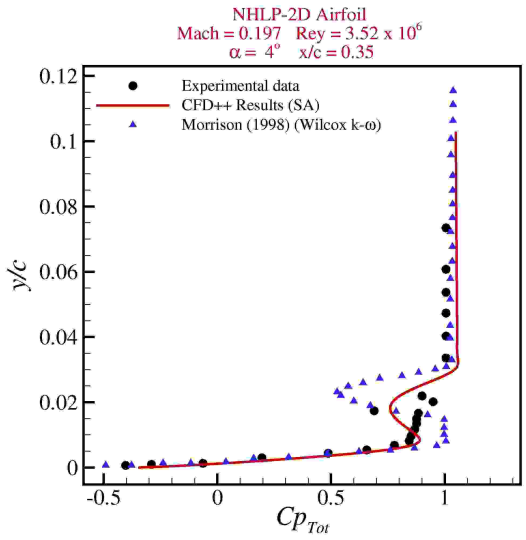

Fig. 12 Total pressure profile at x/c = 0.35.

location is predicted very similarly for SA turbulence model, but the wake defect and wake width vary.

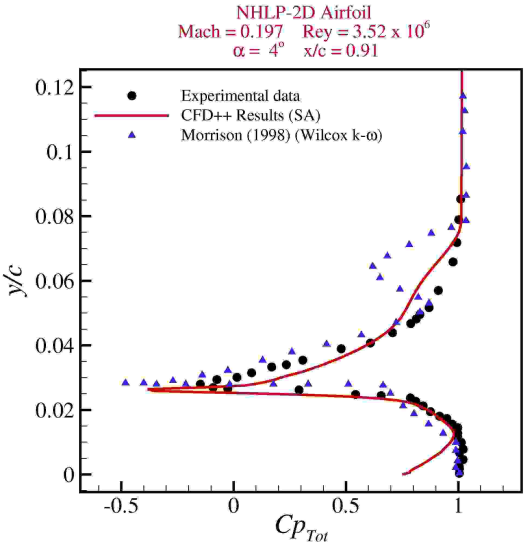

Fig. 13 Total pressure profile at x/c = 0.91.

5 Concluding Remarks

In the present paper, simulation results obtained with SA, SST and $k-\varepsilon$ realizable turbulence models are presented. Two geometries are considered in the present effort. These include a

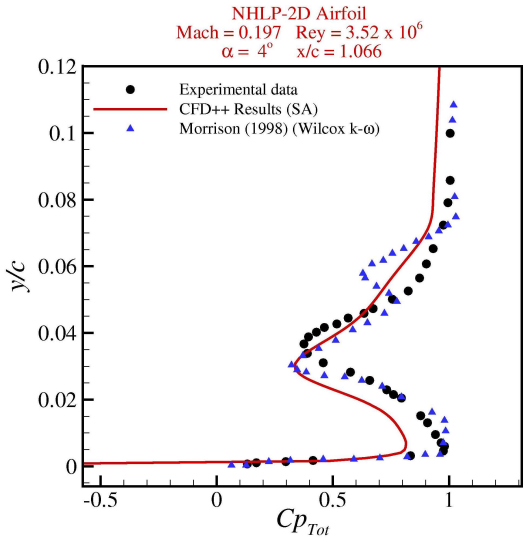

Fig. 14 Total pressure profile at x/c = 1.066.

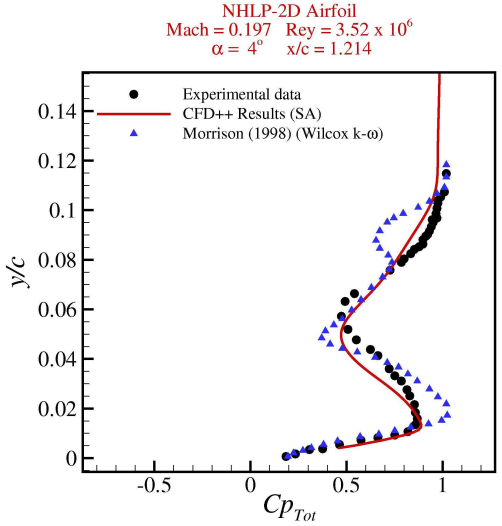

Fig. 15 Total pressure profile at x/c = 1.214.

NLR 7301 airfoil and NHLP-2D airfoil. The paper provides a comparison of the SA, SST and $k-\varepsilon$ realizable turbulence models in the context of two-dimensional high-lift aerodynamic flows. The SA turbulence model is more accurate in attached flows and wakes, including merging boundary layers and wakes. Considering the uncertainties associated with the experimental data and the use RANS approximation, the performance of these SA and SST turbulence models is very good for this application. The SA turbulence model is preferred for general computations of aerodynamic flows, whereas the SST turbulence model is the better choice if separated are of primary interest.

6 Acknowledgments

The authors gratefully acknowledge the support of Fundação de Amparo à Pesquisa do Estado de São Paulo through a Masters Scholarship for the first author under the Fundação de Amparo à Pesquisa do Estado de São Paulo Grant No. 05/57867-0. The authors also acknowledge the partial support of Conselho Nacional de Desenvolvimento Científico e Tecnológico, CNPq, through the Integrated Project Research Grants No. 501200/2003-7.

7 References

[1] “ANSYS ICEM CFD”, Reference Manual, ANSYS INC., 2005.

[2] Van den Berg, B., and Gooden, J.H.M., “Low-Speed Surface Pressure and Boundary Layer Measurement Data for the NLR 7301 Airfoil Section With Trailing Edge Flap”, *A Selection of Experimental Test Cases for the Validation of CFD Codes - AGARD AR-303*, vol. 2, pp. A9-1–A9-12, 1994.

[3] Moir, I. R. M., “Measurements on a Two-Dimensional Aerofoil With High-Lift Devices”, *A Selection of Experimental Test Cases for the Validation of CFD Codes - AGARD-303*, vol. 2, pp. A2-1–A2-12, 1994.

[4] Drela, M., “A User’s Guide to MSES 2.92”, MIT Computational Aerospace Sciences Laboratory, 1996.

[5] White, F. M., “*Viscous Fluid Flow*”, McGraw-Hill International Editions, Second edition, 1991.

[6] “The CFD++ Computational Fluid Dynamics Software”, Metacomp Technologies, Inc., West-

lake, CA, 2005.

[7] Lima e Silva, A.L.F., Oliveira Neto, J. A., Antunes, A. P., Mendonça, M. T., Azevedo, J.L.F., and Silveira Neto, A., "Numerical Study of Two-Dimensional High-Lift Configurations Using the MSES Code", *Proceedings of the 18th International Congress of Mechanical Engineering - COBEM 2005*, Ouro Preto, MG, Brazil, Nov. 2005.

[8] Morrison, J. H., "Numerical Study of Turbulence Model Predictions for the MD 30P/30N and NHLP-2D Three-Element High-lift Configurations", *NASA/CR-1998-208967*, 1998.

8 Copyright Statement